A BOUNDARY ELEMENT METHOD FOR POISSON'S EQUATION

by
Stephen V. Harren
http://www.harren.us

1. Poisson's Equation

Figure 1 below depicts a film (*e.g.,* a soap film) on a rim being deflected by a transverse pressure loading p. In the figure, A is the plane of the rim, and t is the tangential length coordinate around the rim measured in the counterclockwise sense. A side view of Fig. 1 is shown in Fig. 2, where T is the surface

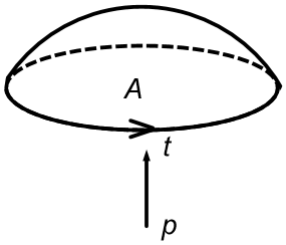

Figure 1. Schematic of a (deflected) film subjected to a pressure loading.

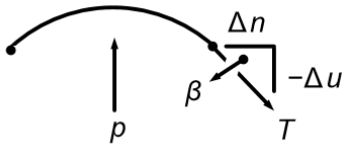

Figure 2. A side view of the film in Fig. 1.

tension of the film (force per unit length). From Fig. 2, for small transverse deflections u,

$$\tan\beta \approx \sin\beta \approx \beta = -\frac{\Delta u}{\Delta n} = -u_{,n} \ , \tag{1}$$

where n is the outward-pointing normal coordinate to the rim, and the comma represents differentiation with respect to that coordinate. Transverse equilibrium is then

$$T \oint_t \sin\beta \, \mathrm{d}t \approx -T \oint_t u_{,n} \mathrm{d}t = \int_A p \mathrm{d}A \ , \tag{2}$$

or via the Divergence Theorem,

$$-T \int_A u_{,ii} \mathrm{d}A = \int_A \mathrm{p} dA \tag{3}$$

so that the governing equation for the deflection of the film is

$$T u_{,ii} + p = 0 \quad \text{or} \quad T\nabla^2 u + p = 0 \ , \tag{4}$$

which is Poisson's equation (and ∇^2 is the Laplacian operator). In rectangular coordinates

$$\nabla^2 u = u_{,xx} + u_{,yy} \ , \tag{5}$$

and in polar coordinates

$$\nabla^2 u = u_{,rr} + \frac{1}{r} u_{,r} + \frac{1}{r^2} u_{,\theta\theta} \ . \tag{6}$$

2. Example in Rectangular Coordinates

Consider the $L \times H$ rectangular domain, pictured in Fig. 3, subjected to the "bubble" pressure distribution

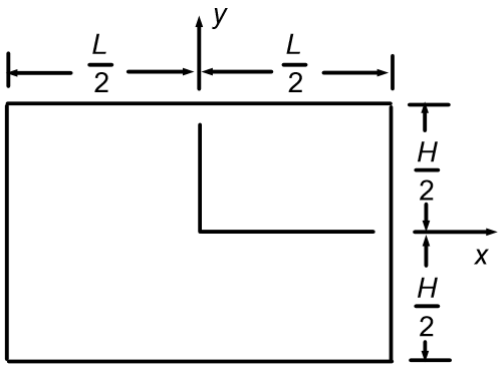

Figure 3. Rectangular domain as described in the text.

$$p = p_0 \cos\left(\frac{\pi x}{L}\right) \cos\left(\frac{\pi y}{H}\right), \tag{7}$$

where p_0 is the pressure at the origin. The boundary conditions are

$$u = 0 \tag{8}$$

on all four faces. Here, the governing equation is, *cf.,* eqns. (4) and (5) of **§1**,

$$u_{,xx} + u_{,yy} = -\frac{1}{T} p_0 \cos\left(\frac{\pi x}{L}\right) \cos\left(\frac{\pi y}{H}\right). \tag{9}$$

Equation (9) is solved with a displacement of the form

$$u = k \cos\left(\frac{\pi x}{L}\right) \cos\left(\frac{\pi y}{H}\right). \tag{10}$$

Note that eqn. (10) satisfies the boundary conditions (8). In any case, substituting eqn. (10) into eqn. (9) yields the value of k, *viz.,*

$$k = \frac{p_0}{\pi^2 T}\left(\frac{L^2 H^2}{L^2 + H^2}\right). \tag{11}$$

Also, the gradients are

$$u_{,x} = -k\frac{\pi}{L}\sin\left(\frac{\pi x}{L}\right)\cos\left(\frac{\pi y}{H}\right), \qquad u_{,y} = -k\frac{\pi}{H}\cos\left(\frac{\pi x}{L}\right)\sin\left(\frac{\pi y}{H}\right). \tag{12}$$

3. Example in Polar Coordinates

Consider the quarter-annular domain shown in Fig. 4 subjected to the pressure load

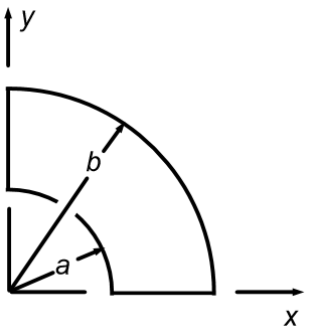

Figure 4. Quarter-annular domain as described in the text.

$$p = \frac{2F}{b^2 - a^2}\cos\theta, \tag{13}$$

where F is the net force acting on the domain, *i.e.,*

$$F = \int_A p \mathrm{d}A. \tag{14}$$

In this case the governing equation is

$$u_{,rr} + \frac{1}{r}u_{,r} + \frac{1}{r^2}u_{,\theta\theta} = -\frac{2F}{T(b^2 - a^2)}\cos\theta, \tag{15}$$

cf., eqns. (4) and (6) of **§1**. The boundary conditions for the problem are

$$u_{,n} = 0 \text{ on } \theta = 0, \quad \text{and} \quad u = 0 \text{ on the other three boundaries.} \tag{16}$$

Assuming a displacement of the form

$$u = f(r)\cos\theta \tag{17}$$

eqn. (15) becomes

$$f'' + \frac{1}{r}f' - \frac{1}{r^2}f = -\frac{2F}{T(b^2 - a^2)}\,, \tag{18}$$

whose general solution is

$$f = k_1 r + \frac{k_2}{r} - \frac{2F}{3T(b^2 - a^2)}r^2\ , \qquad f' = k_1 - \frac{k_2}{r^2} - \frac{4F}{3T(b^2 - a^2)}r\,. \tag{19}$$

Also, the components of the gradient are

$$(\boldsymbol{\nabla} u)_r = u_{,r} = f'(r)\cos\theta\ , \qquad (\boldsymbol{\nabla} u)_\theta = \frac{1}{r}u_{,\theta} = -\frac{1}{r}f(r)\sin\theta\ . \tag{20}$$

Finally, one notes, from eqns. (17) and (20), that the boundary conditions are satisfied identically on the faces $\theta = 0$ and $\theta = \pi/2$. Then, satisfying the boundary conditions on $r = a$ and $r = b$ gives the values of the constants

$$k_1 = \frac{2F(b^3 - a^3)}{3T(b^2 - a^2)^2}\ , \qquad k_2 = -\frac{2Fa^2b^2(b - a)}{3T(b^2 - a^2)^2}\ , \tag{21}$$

which solves the problem at hand.

4. The Green's Function

Let g be the transverse displacement due to a unit point load applied to the film in the transverse direction at the origin of the coordinate system. The function g is termed the Green's function. The

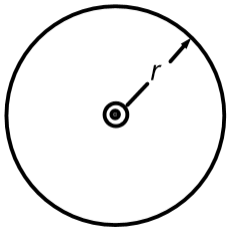

Figure 5. Unit point load applied at the origin of the coordinate system.

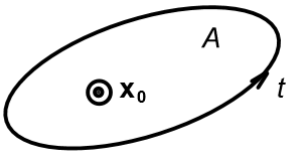

Figure 6. Translation of the unit point load to the point $\mathbf{x}_0$.

Green's function satisfies $\nabla^2 g = 0$ with $g = g(r)$ only. Via eqn. (6) of **§1** then

$$g'' + \frac{1}{r}g' = 0\,. \tag{22}$$

The solution to eqn. (22) of interest is

$$g = k\ln r\ . \tag{23}$$

Enforcing equilibrium with the point load gives, *cf.,* Fig. 5,

$$T\int_0^{2\pi} g_{,r}r\,\mathrm{d}\theta = -1 \quad \Rightarrow \quad k = -\frac{1}{2\pi T}\,. \tag{24}$$

Next, the unit point load is translated to the point $\mathbf{x}_0$ as depicted in Fig. 6. Denoting

$$X_i = x_i - x_{0i} \ , \qquad r = \sqrt{X_i X_i} \ , \tag{25}$$

the Green's function becomes

$$g = -\frac{1}{2\pi T} \ln r . \tag{26}$$

Using $r_{,i} = X_i / r$, the normal derivative of g is

$$g_{,n} = n_i g_{,i} = -\frac{1}{2\pi T} \frac{(\mathbf{n} \cdot \mathbf{X})}{r^2} , \tag{27}$$

where $\mathbf{n}$ is the outward-pointing unit normal vector on the boundary of the domain shown above in Fig. 6. Now, via the Divergence Theorem,

$$T \int_A g_{,ii} \mathrm{d}A = T \oint_t g_{,n} \mathrm{d}t = -\gamma \quad \text{where} \quad \gamma = \begin{bmatrix} 1 \text{ if } \mathbf{x}_0 \text{ is in } A \\ 0 \text{ if } \mathbf{x}_0 \text{ is outside of } A \end{bmatrix} . \tag{28}$$

Since $g_{,ii} = 0$ everywhere, except at $\mathbf{x}_0$ where it is singular, eqn. (28) gives

$$T \int_A u g_{,ii} \mathrm{d}A = -\gamma u(\mathbf{x}_0) , \tag{29}$$

where u is a non-singular transverse displacement.

Finally, in what follows, the derivatives with respect to $\mathbf{x}_0$ will be required. Using the notation

$$\frac{\partial f}{\partial x_{0i}} \equiv f_{:i} \quad \Rightarrow \quad X_{i:j} = -\delta_{ij} , \qquad r_{:i} = -\frac{X_i}{r} \ , \tag{30}$$

where δ_{ij} is the Kronecker delta (or identity matrix), one obtains the derivatives

$$g_{:i} = \frac{1}{2\pi T} \frac{X_i}{r^2} \ , \qquad g_{,n:i} = \frac{1}{2\pi T} \left[\frac{n_i}{r^2} - 2(\mathbf{n} \cdot \mathbf{X}) \frac{X_i}{r^4} \right] . \tag{31}$$

5. The Reciprocal Theorem

The governing equation is $T u_{,ii} = -p$, or by multiplying by g,

$$T g u_{,ii} = -gp . \tag{32}$$

By the product rule of differentiation, $g u_{,ii} = \left(g u_{,i}\right)_{,i} - g_{,i} u_{,i}$. Thus, eqn. (32) becomes

$$T \left(g u_{,i}\right)_{,i} - T g_{,i} u_{,i} = -gp . \tag{33}$$

Using the product rule of differentiation again, $g_{,i} u_{,i} = \left(g_{,i} u\right)_{,i} - g_{,ii} u$, then eqn. (33) gives

$$T \left(g u_{,i}\right)_{,i} - T \left(g_{,i} u\right)_{,i} + T g_{,ii} u = -gp. \tag{34}$$

Integrating eqn. (34) over the domain A and using the Divergence Theorem, one obtains

$$T \oint_t g_{,n} u \mathrm{d}t - T \oint_t g u_{,n} \mathrm{d}t - \int_A gp \mathrm{d}A = T \oint_A g_{,ii} u \mathrm{d}A . \tag{35}$$

Finally, via eqn. (29) of **§4**, eqn. (35) becomes

$$\gamma u(\mathbf{x}_0) = T \oint_t g u_{,n} \mathrm{d}t - T \oint_t g_{,n} u \mathrm{d}t + \int_A g p \mathrm{d}A \,, \tag{36}$$

which is the Reciprocal Theorem, and is the basis of the Boundary Element Method. The gradient of eqn. (36) with respect to $\mathbf{x}_0$ is also useful, *viz.,* for $\gamma = 1$ ($\mathbf{x}_0$ is in A),

$$u_{,i}(\mathbf{x}_0) = T \oint_t g_{,i} u_{,n} \mathrm{d}t - T \oint_t g_{,ni} u \mathrm{d}t + \int_A g_{,i} p \mathrm{d}A \,. \tag{37}$$

6. Integration Cell

The integrals over the domain A in eqns. (36) and (37) are performed numerically using the integration cell depicted at left in Fig. 7, which is in normalized $\boldsymbol{\xi}$–space spanning $(-1,1) \times (-1,1)$. The geometry of the cell in physical $\mathbf{x}$–space is interpolated with the aid of the quadratic functions

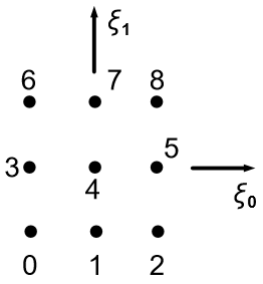

Figure 7. Cell used to perform the numerical area integrations.

$$\begin{aligned} a^0 &= \frac{1}{2}(-\xi + \xi^2) \\ a^1 &= 1 - \xi^2 \\ a^2 &= \frac{1}{2}(\xi + \xi^2) \,, \end{aligned} \tag{38}$$

the tensor product of which functions yield the desired interpolation functions S^I, *viz.,*

$$\begin{array}{lll} S^0 = a^0(\xi_0)a^0(\xi_1) & S^1 = a^1(\xi_0)a^0(\xi_1) & S^2 = a^2(\xi_0)a^0(\xi_1) \\ S^3 = a^0(\xi_0)a^1(\xi_1) & S^4 = a^1(\xi_0)a^1(\xi_1) & S^5 = a^2(\xi_0)a^1(\xi_1) \\ S^6 = a^0(\xi_0)a^2(\xi_1) & S^7 = a^1(\xi_0)a^2(\xi_1) & S^8 = a^2(\xi_0)a^2(\xi_1) \end{array} \,, \tag{39}$$

which are the usual "shape" functions of the 9–node LaGrange finite element. Notwithstanding, the physical coordinates and pressure are interpolated via

$$x_i = S^I x_i^I \,, \qquad p = S^I p^I \,, \tag{40}$$

where x_i^I are the physical coordinates of the integration cell points, and p^I are the pressures at those points. Now, differentiation of the first of eqns. (40) gives

$$\frac{\partial x_i}{\partial \xi_\alpha} = S^I_{,\alpha} x_i^I \equiv A_{i\alpha} \,, \qquad \mathrm{d}x_i = A_{i\alpha} \mathrm{d}\xi_\alpha \,, \qquad \mathrm{d}A_{\mathbf{x}} = (\det A_{i\alpha}) \mathrm{d}A_{\boldsymbol{\xi}} \,, \tag{41}$$

where $\mathrm{d}A_{\mathbf{x}}$ is the differential of area in $\mathbf{x}$–space, and $\mathrm{d}A_{\boldsymbol{\xi}}$ is the differential of area in $\boldsymbol{\xi}$–space. Thus,

$$\int_{A_{\mathbf{x}}} f \mathrm{d}A_{\mathbf{x}} = \int_{A_{\boldsymbol{\xi}}} f \, (\det A_{i\alpha}) \mathrm{d}A_{\boldsymbol{\xi}} \,. \tag{42}$$

The integration (42) is carried out numerically via a Gauss-Legendre quadrature rule.

7. A Five Degree-of-Freedom Curved Boundary Element

7.1. Element Geometry and Interpolations

The boundary element is pictured below in Figs. 8 and 9. The displacement u is interpolated via

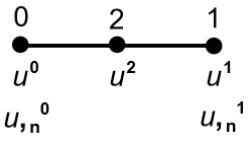

Figure 8. Degrees-of-freedom of the boundary element.

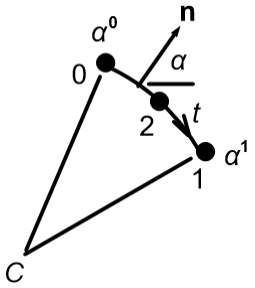

Figure 9. The curved version of the boundary element.

$$u = a^0 u^0 + a^1 u^2 + a^2 u^1 \,, \tag{43}$$

where the functions a^I are given by eqns. (38) of **§6**. Note that along the element $\xi \in (-1,1)$ and $t \in (0, L)$, where L is the length of the element. The mid-node 2 of the element is located at $\xi = 0$, or equivalently, at $t = L/2$. While u is interpolated as being quadratic, the normal derivative $u_{,n}$ is interpolated as being linear, *viz.,*

$$u_{,n} = b^0 u^0_{,n} + b^1 u^1_{,n} \,, \qquad b^0 = \frac{1}{2}(1-\xi) \,, \qquad b^1 = \frac{1}{2}(1+\xi) \,. \tag{44}$$

Now, the outward-pointing unit normal vector is given by

$$\mathbf{n} = \cos\alpha\, \mathbf{e}_x + \sin\alpha\, \mathbf{e}_y \,, \tag{45}$$

where $\mathbf{e}_x$ and $\mathbf{e}_y$ are the Cartesian base vectors. The angle is interpolated through the element as

$$\alpha = b^0 \alpha^0 + b^1 \alpha^1 \,, \tag{46}$$

where α^I are the nodal values of the angle.

The element may either be straight or curved. If it is straight, then

$$\alpha \equiv \text{constant} \,, \qquad x_i = b^I x^I_i \,, \qquad L = \sqrt{(x^1_0 - x^0_0)^2 + (x^1_1 - x^0_1)^2} \,. \tag{47}$$

The quantities x^I_i (node $I = 0,1$) are the nodal coordinates of the element. If the element is curved, as pictured in Fig. 9, then $\alpha_{,t} = c \equiv \text{constant}$, *i.e.,* it has constant curvature c (it is a circular arc with center of curvature C in Fig. 9). Note that curvature may be positive or negative. Notwithstanding, in this case the interpolations are

$$c = \frac{\cos\alpha^1 - \cos\alpha^0}{x^1_0 - x^0_0} \text{ or } c = \frac{\sin\alpha^1 - \sin\alpha^0}{x^1_1 - x^0_1} \,, \quad L = \frac{\alpha^1 - \alpha^0}{c} \,, \quad x_0 = \frac{\cos\alpha}{c} \,, \quad x_1 = \frac{\sin\alpha}{c} \,. \tag{48}$$

The interpolations (43) and (44) may be written as

$$v^I = \begin{bmatrix} u^0 \\ u^0_{,n} \\ u^2 \\ u^1 \\ u^1_{,n} \end{bmatrix} = \begin{bmatrix} v^0 \\ v^1 \\ v^2 \\ v^3 \\ v^4 \end{bmatrix}, \qquad A^I = \begin{bmatrix} a^0 \\ 0 \\ a^1 \\ a^2 \\ 0 \end{bmatrix}, \qquad B^I = \begin{bmatrix} 0 \\ b^0 \\ 0 \\ 0 \\ b^1 \end{bmatrix}, \qquad u = A^I v^I, \qquad u_{,n} = B^I v^I. \tag{49}$$

7.2. Boundary Values Solution

Substituting the interpolations (49) into eqn. (36) of **§5**, with $\gamma = 0$ for $\mathbf{x}_0$ outside of A, one obtains the relationship for the element

$$K^I v^I = M, \qquad K^I = T\int_0^L \left(g_{,n}A^I - gB^I\right)\mathrm{d}t, \qquad M = \int_A gp\mathrm{d}A. \tag{50}$$

The integrals over the length of the element are performed using Gauss-Legendre quadrature with

$$\int_0^L f\mathrm{d}t = \frac{L}{2}\int_{-1}^{1} f\mathrm{d}\xi. \tag{51}$$

Assembling eqn. (50) over all the boundary elements of the discretized boundary gives a system of equations relating all the degrees-of-freedom on the boundary. The boundary conditions for the problem need to be applied to this system to obtain equations which may be solved for the unknown boundary values. The two cases of admissible boundary conditions are listed below in the table.

Case	Prescribed	Unknown
0	u	$u_{,n}$
1	$u_{,n}$	u

For each unknown boundary value, a singularity $\mathbf{x}_0$ is placed near its boundary node to generate a single equation. Traditionally, the singularity is placed on the boundary node, but for more complicated systems of partial differential equations, this choice can be problematical. Consequently, here it is chosen to place the singularity outside of the domain A near the boundary node as depicted in Figs. 10 and 11 below. In these figures the prescribed boundary values are indicated in red, and the red points indicate the placement of the singularities.

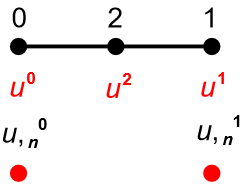

Figure 10. Boundary condition case 0 as described in the text.

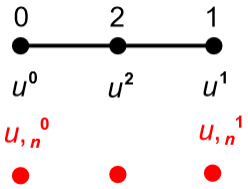

Figure 11. Boundary condition case 1 as described in the text.

Again, once the boundary conditions are applied, the resulting system may be solved for the unknown boundary values.

7.3. Calculation of Gradients on the Boundary

Having all the boundary values known, the gradients $u_{,i}$ on the boundary may be calculated as

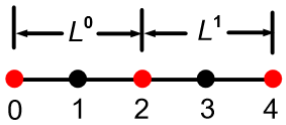

Figure 12. Adjoining boundary elements.

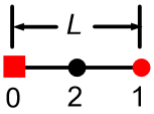

Figure 13. Boundary element after a corner.

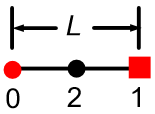

Figure 14. Boundary element before a corner.

follows. When discretizing the boundary, nodes on the corners are double nodes, with one adjoining element belonging to one face, and the other element belonging to the other face. In the calculations, the continuity of the corner displacements u is not directly enforced for the two elements adjoining the corner, but in the numerical solution they come out to be continuous for all practical purposes. Notwithstanding, in Figs. 12 through 14 above, the red nodes are nodes 0 and 1 of each element, and the black nodes are the midpoint node 2. Figure 12 shows two adjoining elements. Here, the tangential gradient at point 2 in the figure is calculated via central difference as

$$u^2_{,t} \approx \frac{u^3 - u^1}{\frac{1}{2}(L^0 + L^1)} . \tag{52}$$

Figure 13 shows the case where a boundary element is directly after a corner. The square node 0 is on a corner, and the gradient at point 0 is calculated with forward difference

$$u^0_{,t} \approx \frac{u^2 - u^0}{\frac{1}{2}L} . \tag{53}$$

Finally, when the element is directly before the corner (Fig. 14, where the square node 1 is on a corner), backward difference is used for node 1, *viz.,*

$$u^1_{,t} \approx \frac{u^1 - u^2}{\frac{1}{2}L} . \tag{54}$$

At this point then, $u_{,t}$ is known at all the major (two degree-of-freedom) nodes, as is $u_{,n}$ (from the element vectors v^I). With obvious notation then, the gradients may be transformed from the nt–system to the xy–system via

$$\psi_{ij} = \begin{bmatrix} \cos\alpha & \sin\alpha \\ -\sin\alpha & \cos\alpha \end{bmatrix}, \qquad u^{xy}_{,j} = u^{nt}_{,i}\psi_{ij} . \tag{55}$$

Once $u^{xy}_{,i}$ is calculated, the values of u and $u^{xy}_{,i}$ are averaged at the corner nodes to enforce continuity.

7.4. Calculation of the Solution Inside of the Domain

The discretized form of eqns. (36) and (37) of **§5** (with $\gamma = 1$ for $\mathbf{x}_0$ in the domain A) are

$$u(\mathbf{x}_0) = M - K^I v^I , \qquad u_{:i}(\mathbf{x}_0) = M_{:i} - K^I_{:i} v^I \tag{56}$$

with

$$K^I_{:i} = T\int_0^L \left(g_{,n:i}A^I - g_{:i}B^I\right)\mathrm{d}t , \qquad M_{:i} = \int_A g_{:i}p\mathrm{d}A . \tag{57}$$

So, by placing a singularity $\mathbf{x}_0$ at each internal point of A in turn, performing the circuit integrals for each placement yields the solution for u and ∇u at each of the internal points. Thus, the entire solution is had.

8. Numerical Example – Rectangular Coordinates

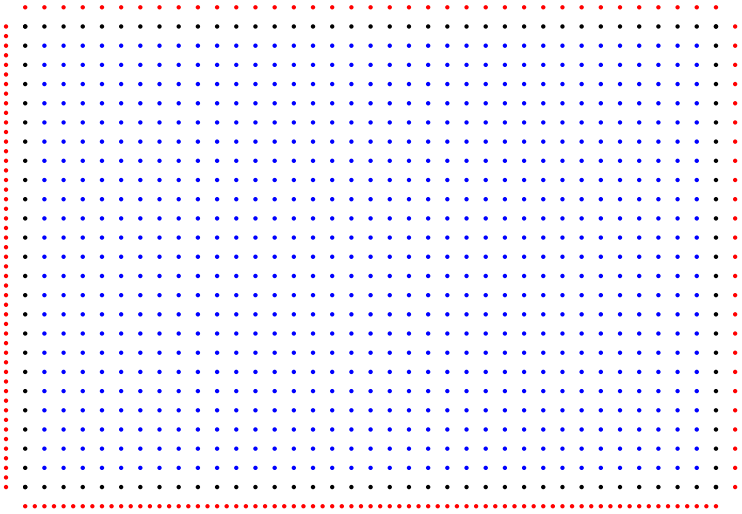

Figure 15. Computational grid used in the analysis as described in the text.

Here the problem solved above in **§2** is solved numerically. Owing to symmetry, only the upper right quadrant of the domain A in Fig. 3 of **§2** is analyzed. The corresponding boundary conditions are then

$$u = 0 \text{ on } x = \frac{L}{2} \text{ and } y = \frac{H}{2},$$

$$u_{,n} = 0 \text{ on } x = 0 \text{ and } y = 0\,. \quad (58)$$

The constants used in the analysis are

$$L = 12.0 \text{ in}, \qquad H = 8.0 \text{ in}$$

$$p_0 = 5 \times 10^{-3} \text{ psi}, \qquad (59)$$

$$T = 4.14 \times 10^{-4} \text{ lb/in}\,.$$

For lack of a better choice, the constant T in eqns. (59) is for water.

Figure 15 above shows the computational grid used in the analysis. The black and blue points in the grid are a 37×25 array of points. The black points are on the boundary of the domain, and between the black points are the 120 boundary elements (the central node 2 of each boundary element is not shown). Also, the black points on the corners are double nodes. The 805 blue points are in the interior of the domain. The domain is spanned by an 18×12 array of 216 integration cells, *cf.,* **§6**. The resulting system to solve consists of 368 degrees-of-freedom with 184 equations. The 184 red points in the figure are where the singularity points $\mathbf{x}_0$ are placed to generate the equations. Finally, all integrations are performed with the 16–point (or 16×16 point) Gauss-Legendre quadrature rule.

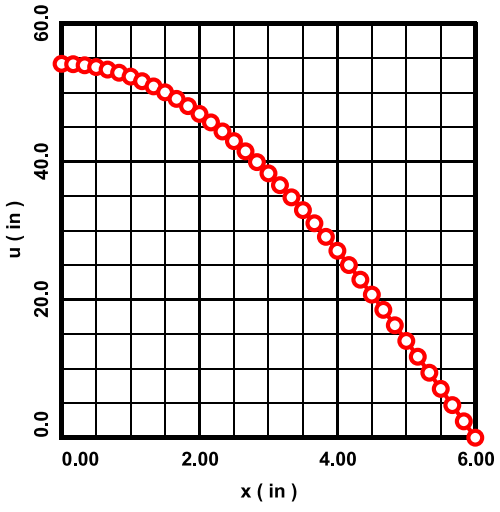

Figure 16. Exact and numerical results for displacement u along $y = 0$.

Figure 16 at left shows the exact (solid curve) and numerical (plotted points) solutions for the displacement u along the bottom surface of the domain. The displacements are from the boundary element vector v^I, *cf,* eqn. (49) of **§7**. For all practical purposes, the numerical method reproduces the exact solution. Figure 17 below shows the results for the displacement gradient $u_{,x}$ also along the bottom surface. As described in *§7.3*, the numerical results in Fig. 17 are calculated by a finite difference procedure. Once again, the numerical results basically reproduce the exact solution.

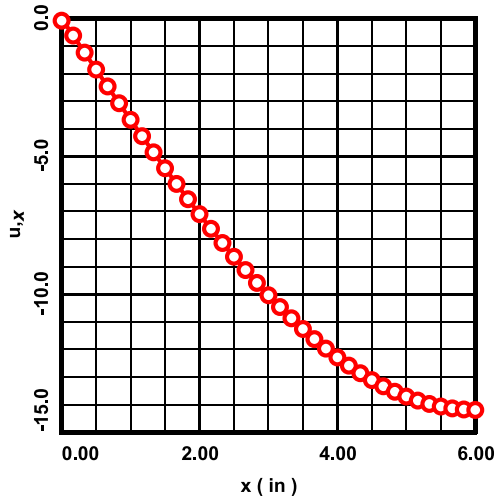

Figure 17. Exact and numerical results for displacement gradient $u_{,x}$ along $y = 0$.

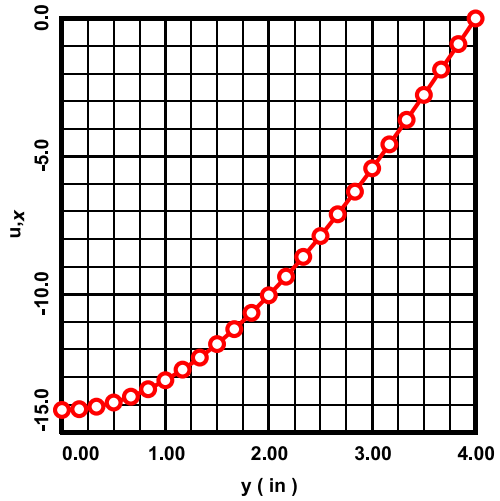

Figure 18. Exact and numerical results for displacement gradient $u_{,x}$ along $x = 6$ in.

Figure 18 at above right shows the results for $u_{,x}$ along the right face of the domain. The numerical results are from the boundary element vector v^I, and as before, the exact solution essentially is reproduced.

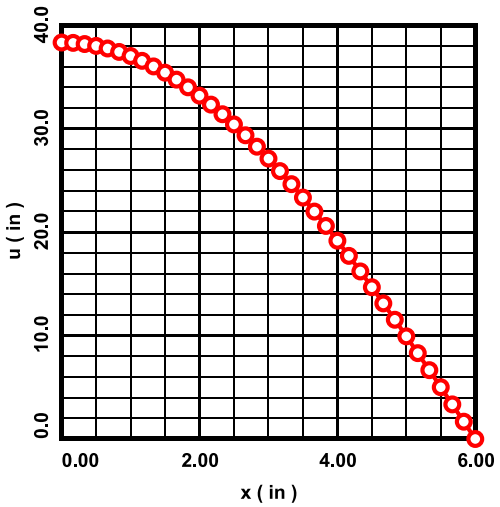

Figure 19. Exact and numerical results for displacement u along $y = 2$ in.

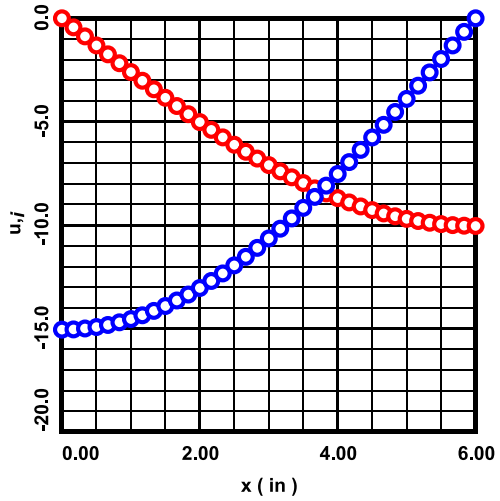

Figure 20. Exact and numerical results for displacement gradients $u_{,x}$ (red) and $u_{,y}$ (blue) along $y = 2$ in.

Figures 19 and 20 above show results from along the horizontal line $y = H/2$ running through the interior of the domain. Once again, the exact and numerical solutions basically coincide.

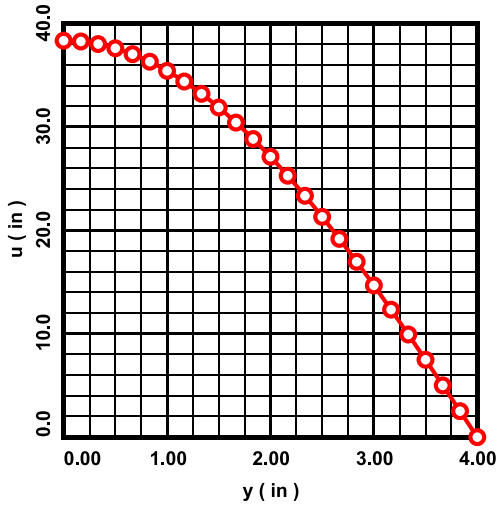

Figure 21. Exact and numerical results for displacement u along $x = 3$ in.

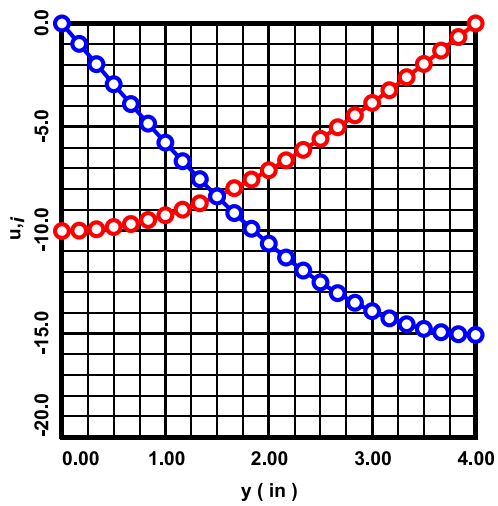

Figure 22. Exact and numerical results for displacement gradients $u_{,x}$ (red) and $u_{,y}$ (blue) along $x = 3$ in.

Finally, Figs. 21 and 22 above show results from along the vertical line $x = L/2$ running through the interior of the domain. As previously, the numerical results are highly accurate.

9. Numerical Example – Polar Coordinates

Here, the problem solved previously in **§3** is analyzed numerically. The domain analyzed is that of Fig. 4 of **§3**. The constants used for the analysis are

$$a = 6.0 \text{ in}, \qquad b = 12.0 \text{ in}, \qquad F = 2.0 \text{ lb}, \qquad T = 4.14 \times 10^{-4} \text{ lb/in}. \tag{60}$$

The computational grid used for the calculations is shown below in Fig. 23. The black and blue points in the figure are a 25 (radial) by 37 (tangential) array of points. The black points are on the boundary of the domain, and between the black points run 120 boundary elements. Note that the midpoint nodes 2 of the boundary elements are not shown. The 805 blue points are in the interior of the domain. Also, the domain is spanned by a 12 (radial) by 18 (tangential) array of 216 integration cells, *cf.,* **§6**. The resulting system contains 368 degrees-of-freedom with 148 equations. The 148 red points in the figure are where the singularities $\mathbf{x}_0$ are placed to generate the necessary equations. Finally, the integrations were carried out using the 24–point (or 24×24 point) Gauss-Legendre quadrature rule.

Figure 24 below shows the exact solution (solid curve) and numerical results (plotted points) for the displacement u along the boundary $\theta = 0$. The numerical results are from the element vectors v^I, *cf.,* eqn. (49) of **§7**. As is evident, the numerical results are highly accurate.

Figure 25 below shows the exact and numerical results for the normal derivative $u_{,n}$ along the outer boundary $r = b$. Once again, the numerical results are from the solution vector v^I, and the numerical results are very accurate.

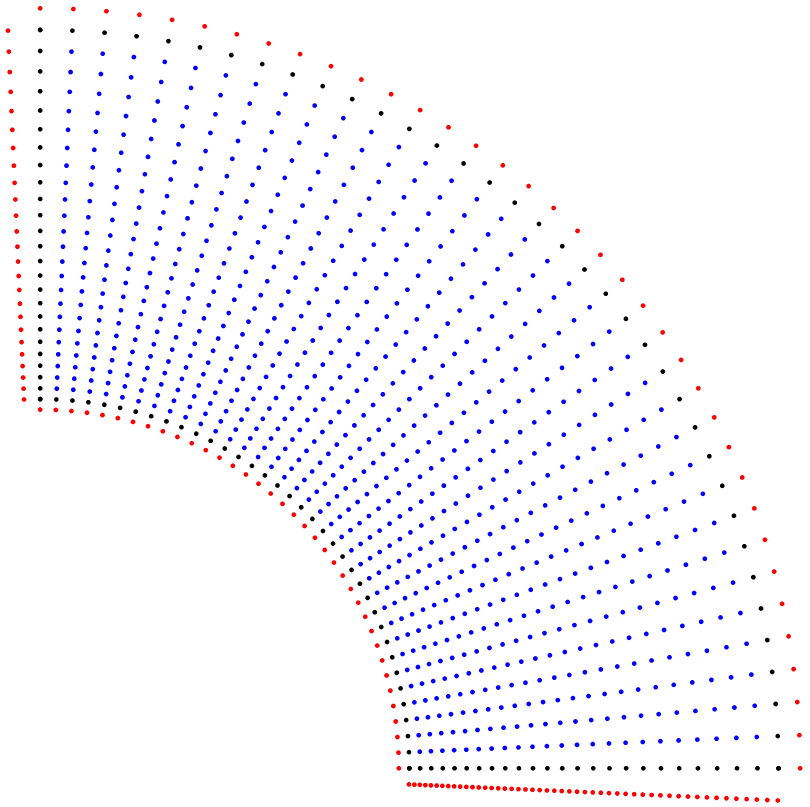

Figure 23. Computational grid used in the analysis as explained in the text.

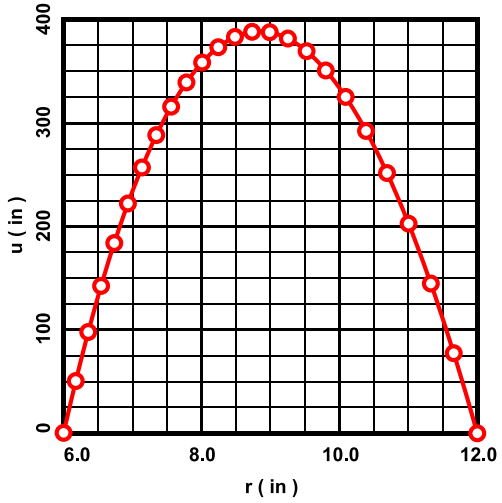

Figure 24. Exact and numerical results for displacement u at $\theta = 0$.

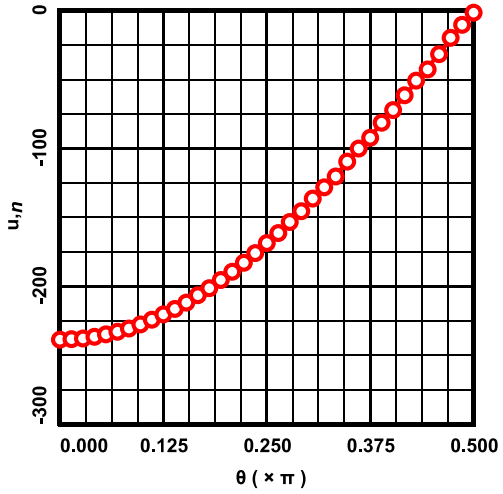

Figure 25. Exact and numerical results for normal derivative $u_{,n}$ at $r = b$.

Figure 26 below shows the results for the normal derivative $u_{,n}$ on the boundary located at $\theta = \pi/2$. As before, the numerical results are from the vector v^I. Except for the single point at $r = b$, the numerical results again are accurate.

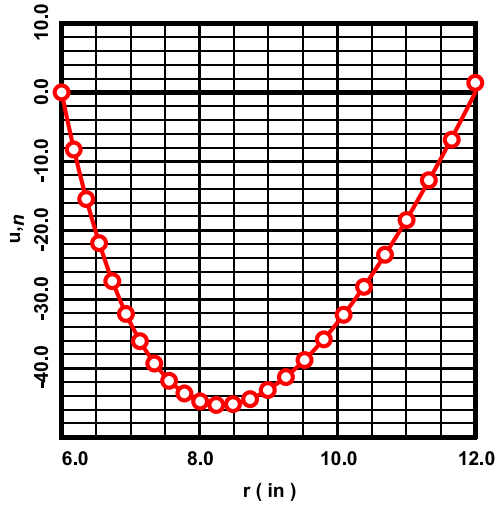

Figure 26. Exact and numerical results for normal derivative $u_{,n}$ at $\theta = \pi/2$.

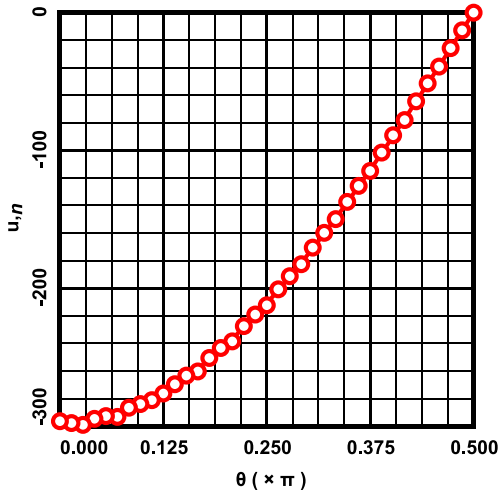

Figure 27. Exact and numerical results for normal derivative $u_{,n}$ at $r = a$.

Figure 27 above shows the results for the normal derivative $u_{,n}$ on the boundary located at $r = a$. Again, the numerical results are from v^I. While the magnitudes of the numerically calculated points are accurate, there are slight oscillations exhibited by the numerical solution on $\theta \in (0, \pi/4)$. This is the least accurate part of the solution, and this behavior will be discussed later in **§10**.

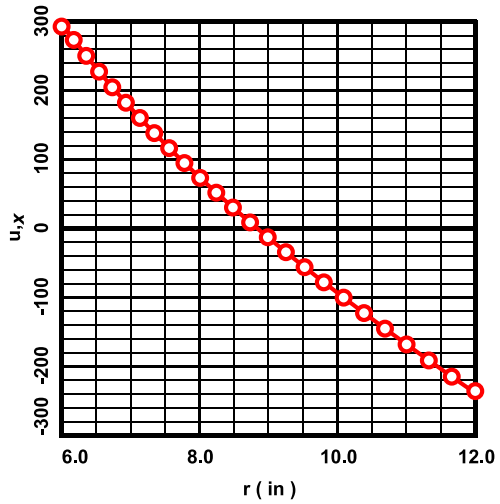

Figure 28. Exact and numerical results for displacement gradient $u_{,x}$ at $\theta = 0$.

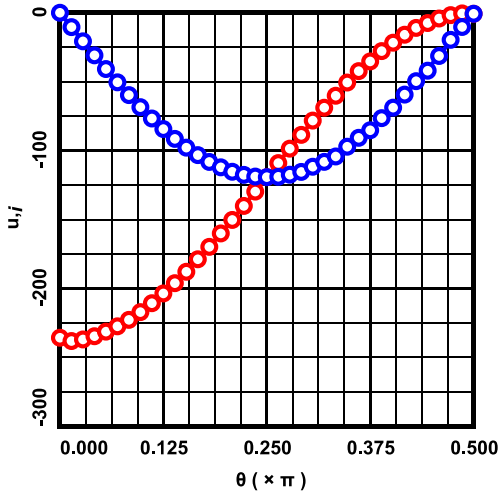

Figure 29. Exact and numerical results for displacement gradients $u_{,x}$ (red) and $u_{,y}$ (blue) at $r = b$.

Figure 28 above shows the results for the displacement gradient $u_{,x}$ on the boundary located at $\theta = 0$. The numerical results were calculated using the finite difference procedure described in *§7.3*. As is evident, the numerical results are highly accurate.

Figure 29 above shows the displacement gradients $u_{,x}$ and $u_{,y}$ on the boundary located at $r = b$. Again, the numerical results were calculated using the finite difference procedure of *§7.3*. All the numerical results are very accurate except for the little blip in $u_{,x}$ near $\theta = 0$, although the magnitude of $u_{,x}$ there is accurate.

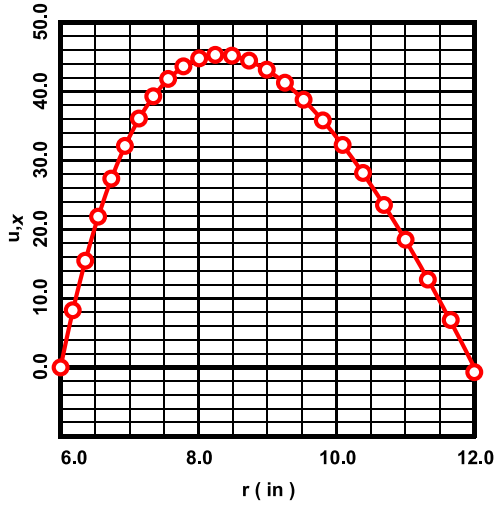

Figure 30. Exact and numerical results for displacement gradient $u_{,x}$ at $\theta = \pi/2$.

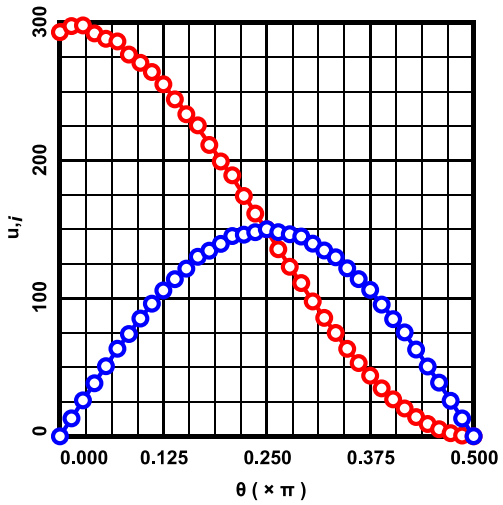

Figure 31. Exact and numerical results for displacement gradients $u_{,x}$ (red) and $u_{,y}$ (blue) at $r = a$.

Figure 30 shows the displacement gradient $u_{,x}$ on the boundary at $\theta = \pi/2$. Except for the sign, these are the same as the results shown in Fig. 26. In Fig. 31 above, the results shown are for the displacement gradients $u_{,x}$ and $u_{,y}$ on the boundary $r = a$. The slight oscillations in $u_{,x}$ on $\theta \in (0, \pi/4)$ are due to those in $u_{,n}$ in Fig. 27. The numerical results for $u_{,y}$ are more accurate, but this component too exhibits small oscillations near $\theta = \pi/4$.

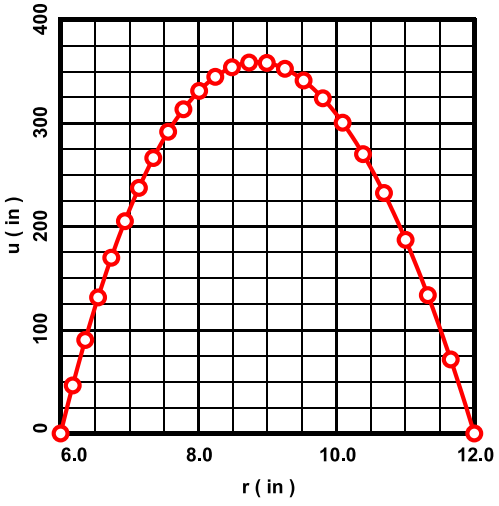

Figure 32. Exact and numerical results for displacement u at $\theta = \pi/8$.

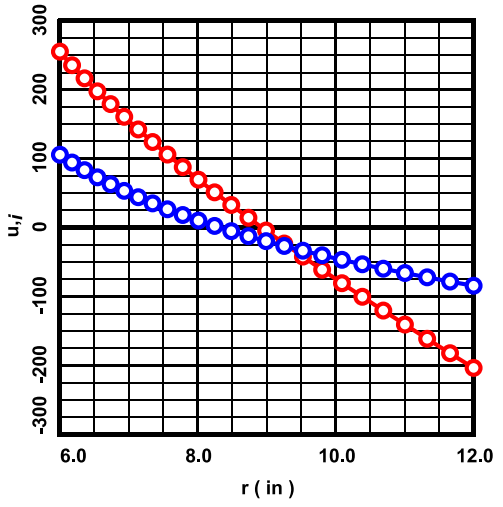

Figure 33. Exact and numerical results for displacement gradients $u_{,x}$ (red) and $u_{,y}$ (blue) at $\theta = \pi/8$.

Figures 32 and 33 above give the results of the numerical calculations for the radial line through the domain at $\theta = \pi/8$. Both the numerical results for the displacement u and the displacement gradients $u_{,x}$ and $u_{,y}$ are highly accurate. Finally, Figs. 34 and 35 below give the calculated results for u, $u_{,x}$ and $u_{,y}$ on the circular arc located at $r = 8.98984$ in in the domain. Once again, the numerically calculated results are highly accurate.

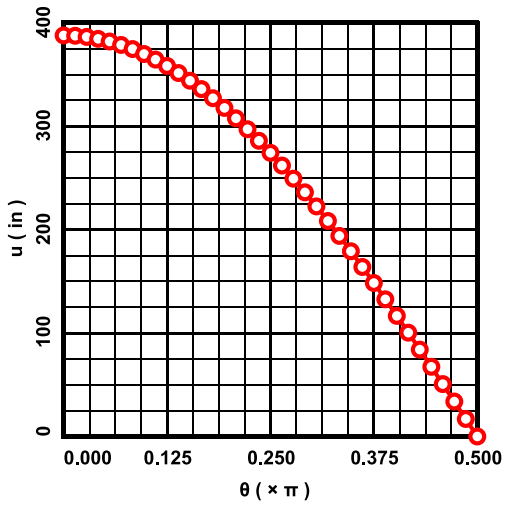

Figure 34. Exact and numerical results for displacement u at $r = 8.98984$ in.

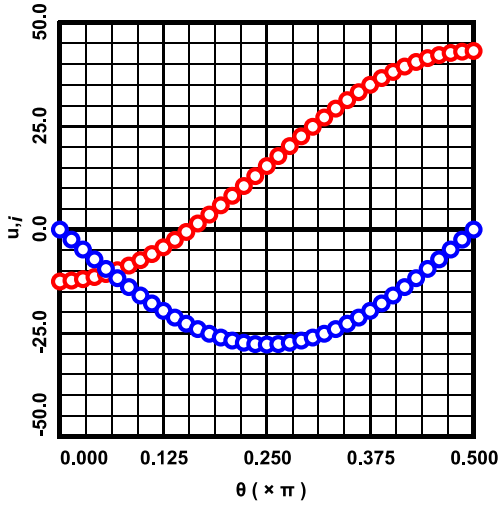

Figure 35. Exact and numerical results for displacement gradients $u_{,x}$ (red) and $u_{,y}$ (blue) at $r = 8.98984$ in.

10. Closing Remarks

A minor comment is that the constants used for the analyses in **§8** and **§9** are unrealistic: they give unrealistically large displacements. Nevertheless, a valid comparison of the numerical method with analytical results has been made.

While completing this work, the author has learned the following. First, it is necessary to interpolate the displacement one order higher than that of the normal derivative. For example, using the same order interpolation for both u and $u_{,n}$ can give oscillatory solutions for the normal derivative, or either the numerical solution which results will not converge to the correct result.

The author has also come to the conclusion that using curved elements is necessary. For instance, for the problem in **§9**, using straight elements (with u interpolated one order higher than $u_{,n}$) gives much more inaccurate solutions, especially for $u_{,n}$.

Finally, the slight oscillations that occur in the solution for the gradient (*cf.,* Figs. 27 and 31 of **§9**) could be the result of a slightly ill-conditioned system, but the author must admit that he has not looked into this.